Flexural-torsional stability of sandwich tapered I-beams with a functionally graded porous core

M. Soltani[*]

Abstract:

The present research deals with the flexural-torsional buckling analysis of sandwich web and/or flanges tapered doubly-symmetric I-beam. All section walls are composed of two metal face layers and a functionally graded (FG) porous core. It is assumed that the material properties of the porous core vary gradually in the longitudinal direction according to the simple power-law function considering the even distribution of porosities. Based on Vlasov's theory for thin-walled cross-section, the governing equations are derived via the energy method. The effect of axial load eccentricity is also considered in the formulation. The differential quadrature method is used to estimate the buckling load. In special cases, the results are compared to other available studies. Then the effects of gradient index, axial load eccentricity, porous coefficient, thickness ratio and tapering parameter on stability behavior of a simply supported three-layered sandwich tapered I-beam with FG porous core are comprehensively assessed. The numerical outcomes of this paper demonstrated that the normalized flexural-torsional buckling load decreases with an increase in the porosity volume fraction.

1. Introduction

Sandwich thin-walled structural components have been applied in aeronautical and mechanical applications, in virtue of their excellent engineering features, such as the low specific density, corrosion resistance, good buckling strength, and good surface finish. Nowadays, the use of multi-layered sandwich members is further enhanced with the development of manufacturing processes and by the introduction of the porous functionally graded materials (FGMs) as the core of sandwich panels. The main reason for this increase is the attractive features of porous FGMs such as thermal resistance, optimal distribution of weight, heat exchange and energy absorbance. Therefore, up to date, several studies have focused on the static, stability and vibration response of FGM and/or homogeneous structural elements with arbitrary cross-sections, a short description of which is presented below.

* *Corresponding Author: Assistant Professor, Department of civil engineering, University of Kashan, Kashan, Iran, E-mail: msoltani@kashanu.ac.ir*

Based on non-linear strain displacement relationship and using the finite element method, Rajasekaran and Nalinaa [1] investigated the vibration and stability analyses of non-prismatic thin-walled composite spatial members of generic section. Samanta and Kumar [2] provided the shell finite element solution for studying the distortional buckling capacity of simply supported beams with mono-symmetric I-section. Machado and Cortinez [3] adopted a geometrically non-linear theory and large displacements and rotations assumptions to investigate the free vibration of composite beams with doubly-symmetric thin-walled open cross-section under static initial stresses and external loading. By considering the impact of the position of transverse load, the distortional and lateral-torsional stability analyses of Light Steel Beams (LSBs) subjected to simply-simply end conditions were studied by Kurniawan and Mahendran [4] through a new finite element methodology. The lateral buckling strength of doubly-symmetric tapered beams subjected to free bending and warping end restrains and the arbitrary bending moment was estimated by Ibanez and Serna [5] via the equivalent moment method. Yuan et al. [6] presented the outcomes of the lateral-torsional buckling of steel Tee-

section beams having linear tapered web subjected to fixed-free end conditions and various transverse loading cases including uniformly distributed force and/or a concentrated one. Additionally, Li et al. [7] exploited the influence of exponential variation of material or geometrical properties on the linear vibration of beams under different end supports. Ebrahimi and Mokhtari [8] inspected the problem of transverse vibration of rotating Timoshenko beam using the differential transform method. Jabbari et al. [9] studied the thermal buckling of a radially solid sandwich circular plate made of a piezoelectric actuator and porous material. Based on the shear deformation theory, the free and forced vibrations of functionally graded porous beams were perused by Chen et al. [10]. In the context of Timoshenko beam theory, Chen at al. [11] assessed the nonlinear free vibration analysis of sandwich beam having a functionally graded porous core using Ritz method and a direct iterative algorithm. Based on Ritz and Galerkin's methods, Saoula et al. [12] studied the stability resistance of laterally unrestrained simply supported thin-walled box beam elements subjected to combined bending and axial forces. Utilizing a Navier solution methodology, the vibrational characteristics of functionally graded (FG) Reddy beams made of porous material loaded by various thermal forces were assessed by Ebrahimi and Jafari [13]. Within the frame of Eringen's nonlocal elasticity theory, Shafiei and Kazemi [14] analyzed the linear buckling behavior of two-dimensional functionally graded tapered beams made of porous materials. Khaniki and Rajasekaran [15] examined the mechanical responses of two-directionally FG microbeam with variable cross-section employing the theory of modified couple stress. Lezgy-Nazargah et al. [16-21] presented some useful work about the analysis of beams with thin-walled cross-section made of functionally graded materials. In the field of functionally graded porous materials, Li at al. [22] employed the generalized differential quadrature method for stability analysis of two-directionally porous beam. Taking into consideration the impact of shear deformation and following Vlasov's assumptions, Nguyen et al. [23] conducted the linear stability and vibration analyses of FG laminated beams with an I-section under different boundary conditions. A finite element approach was recently developed by Koutoati [24] to assess the static and free vibration behaviors of multilayer composite and FG beams through different shear deformation beam theories. Based on Love's shell theory, Ghasemi and Meskini [25] perused the free vibrational characteristics of porous laminated rotating circular cylindrical shells subjected to simply supported boundary conditions via Navier's solution. Achref et al. [26] assessed higher buckling and lateral buckling responses of beams with open cross-sections through an analytical technique and finite element solution. Using a finite element model, a comprehensive investigation on the elastic instability and free vibration behaviors of bi-directional functionally graded tapered thin-walled beams with arbitrary cross-sections was presented by Rajasekaran and Khaniki [27].

As can be seen, the studies in the field of porous materials are exclusively devoted to beams with rectangular cross-section. Hence, there has been no research presented to study the lateral-torsional stability behavior of sandwich doubly-symmetric tapered I-beam having axially functionally graded porous core. Additionally, in previous author's studies, the lateral stability analysis of homogenous beams with variable mono-symmetric cross-section [28], the free vibrational problem and flexural-torsional buckling of non-prismatic beams with thin-walled section [29], steel web and/or flanges tapered beams [30], as well as the lateral buckling problem of tapered I-beams with axially varying materials [31-33] were comprehensively assessed. Due to the application of composite structural members with thin-walled cross-sections in the design of sensitive and modern structures such as aircraft wings, helicopter and turbine blades, it is necessary to study the problem of sandwich laminated thin-walled beams made of porous materials. Motivated by these facts, the main target of the present work is to precisely inspect the influence of porosity on the flexural-torsional buckling behavior of sandwich tapered I-beams having AFG porous core by considering the effects of axial load and bending moment interaction. To this end, the following steps are considered:

Within the framework of Vlasov's model for non-uniform torsion, the coupled fourth-order differential equations for the vertical and lateral deformations as well as the twist angle are acquired using the energy method. It is necessary to note that the compressive axial load and bending moment interaction is also considered in our formulation. It is supposed that all section walls are stacked as steel/ functionally graded porous materials/steel. The material properties of the functionally graded porous core, varies continuously in the longitudinal direction according to the power law model considering the even distribution of porosities. The flexural-torsional buckling load is then estimated for simply supported end conditions with the help of the differential quadrature method. Eventually, a numerical example is provided to investigate the effects of prominent parameters such as power-law index, porosity volume fraction, web and flanges tapering parameters, thickness ratio and axial load positions on the flexural-torsional buckling strength of sandwich thin-walled beams with tapered I-section having a porous core under simply supported boundary conditions.

2. Governing equations

2.1. Axially functionally graded porous material

Through this paper, the linear flexural-torsional buckling analysis is conducted for a sandwich porous I-beam with tapered web and flanges. The right-hand Cartesian co-ordinate system, with x the initial longitudinal axis measured from the left end of the beam, the y-axis in the lateral direction and the z-axis along the vertical direction is considered as indicated in Fig. 1. The origin of these axes (O) is located at the centroid of doubly-symmetric I-section. The sandwich tapered I-beam is subjected to a constant axial load at its ends. To perform the flexural-torsional buckling analysis, the compressive axial force can be applied through an eccentricity from the centroid along the z-axis. It is also assumed that the width of both flanges (b_L) and the web height (d_L) of I-section at the left end are respectively made to increase linearly to $b_R = (1 + \beta_f)b_L$ and $d_R = (1 + \beta_w)d_L$ at the right one. Therefore, the flanges and web tapering ratios are defined as $\beta_f = b_R / b_L - 1$ and $\beta_w = d_R / d_L - 1$, respectively. Note that these two parameters (β_f, β_w) are non-negative variables and can change concurrently or separately. Moreover, by equating these two mentioned parameters (β_f, β_w) to zero, I-beam with uniform cross-section is achieved. As shown in Fig. 1, the thicknesses of the flanges and the web are equal, that is, $t = t_c + 2t_f$, where t_c denotes the core thickness and t_f is the thickness of face layers that are assumed to be perfectly bonded to the core material.

(a)

(b)

I-section at x=0   I-section at x=L   Wall section details

(c)

(d)
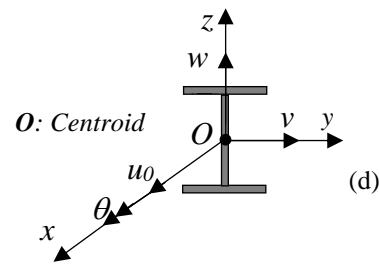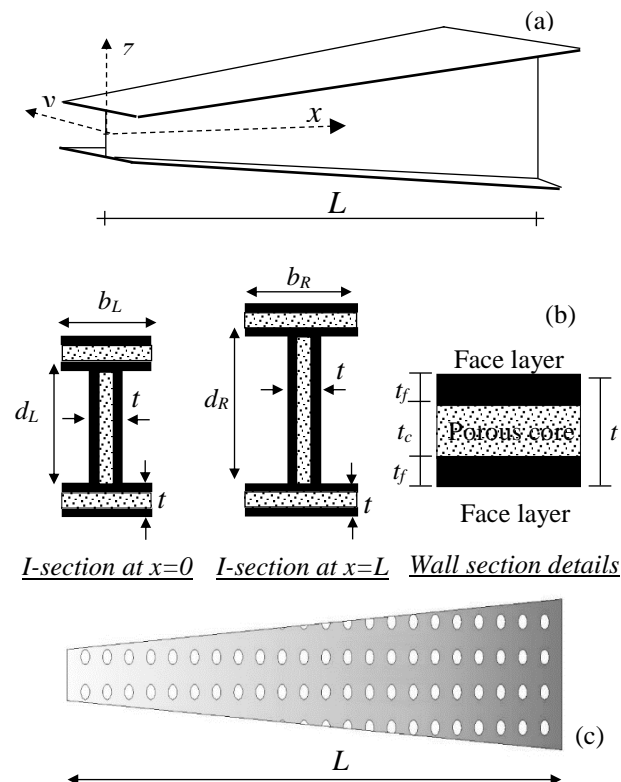
Fig. 1: Beam with variable doubly symmetric I-section: Coordinate system and notation for displacement parameters.

It is assumed that the core of sandwich beam is made of axially varying materials with uniform porosity. Hence, the material features vary along the beam's length from pure ceramic at the left end to pure metal at the right one. FGM possesses characteristics that can be acquired in accordance with the volume fraction of the phase material based on different theories such as: polynomial, exponential, and trigonometric volume fraction laws. Among these functions, power-law distribution [34-35] and exponential function [36-37] are extensively used to describe the material properties variation for FGM. In this study, power-law function is considered to model the material variations.

As mentioned above, the even distribution porosities in the material is considered. Regarding this we have half of the porosity in the ceramic phase and another half in the metal constituents. Under these conditions, the modulus of elasticity of the even porosity type are expressed using Eq. (1) as:

$$E(x) = E_c + (E_m - E_c)(\frac{x}{L})^p - \frac{\alpha}{2}(E_m + E_c) \qquad (1)$$

Here, we use the subscripts of ()$_m$ and ()$_c$ to express the metallic and ceramic phases. α ($\alpha \ll 1$) is the porosity volume fraction. It is to be mentioned that $\alpha = 0$ provides a perfect beam.

2.2. Kinematic relations

In this study, the thin-walled beam with doubly-symmetric I-section is modeled within the framework of Vlasov's thin-walled beam theory for non-uniform torsion. Regarding this theory and following small displacements assumption, the displacement field can be presented as follows:

$$U(x, y, z) = u_0(x) - y\frac{dv(x)}{dx} - z\frac{dw(x)}{dx} \qquad (2a)$$
$$- \omega(y, z)\frac{d\theta(x)}{dx}$$

$$V(x, y, z) = v(x) - z\theta(x) \qquad (2b)$$

$$W(x, y, z) = w(x) + y\theta(x) \qquad (2c)$$

In these equations, U is the axial displacement and displacement components V and W represent lateral and vertical displacements (in direction y and z). The term $\omega(y,z)$ signifies a cross-section variable that is called the warping function, which can be defined based on Saint-Venant's torsion theory and θ is twisting angle.

The Green's strain tensor components which incorporate large displacements including linear and non-linear strain parts are given by:

$$\varepsilon_{ij} = \frac{1}{2}(\frac{\partial U_i}{\partial x_j} + \frac{\partial U_j}{\partial x_i}) + \frac{1}{2}\left(\frac{\partial U_k}{\partial x_i}\frac{\partial U_k}{\partial x_j}\right) = \varepsilon_{ij}^l + \varepsilon_{ij}^* \quad (3)$$
$$i,j,k = x,y,z$$

ε_{ij}^l denotes the linear parts and ε_{ij}^* the quadratic non-linear parts. Using relationships (1-2) and taking into account for tapering, the non-zero linear and non-linear parts of strain displacement are the following:

$$\varepsilon_{xx}^l = u_0' - yv'' - zw'' - \omega\theta'' \quad (4a)$$

$$\gamma_{xz}^l = 2\varepsilon_{xz}^l = \left(y - \frac{\partial\omega}{\partial z}\right)\theta' \quad (4b)$$

$$\gamma_{xy}^l = 2\varepsilon_{xy}^l = -\left(z + \frac{\partial\omega}{\partial y}\right)\theta' \quad (4c)$$

$$\varepsilon_{xx}^* = \frac{1}{2}\left[v'^2 + w'^2 + r^2\theta'^2\right] + yw'\theta' - zv'\theta' \quad (4d)$$

$$\gamma_{xz}^* = -(v' + \theta'z)\theta \quad (4e)$$

$$\gamma_{xy}^* = (w' + \theta'y)\theta \quad (4f)$$

In Eq. (4d), the term r^2 represents $y^2 + z^2$.

In this study, it is contemplated that the concentrated compressive axial load (P) is applied at end beam without an eccentricity from centroid along z-axis. Therefore, an external bending moment occurs about the major principal axis (M_y^*) and the magnitude of bending moment with respect to z-axis (M_z^*) is equal to zero. Regarding this, the most general case of normal and shear stresses associated with the external bending moment M_y^* and shear force V_z are considered as:

$$\sigma_{xx}^0 = \frac{P}{A} - \frac{M_y^*}{I_y}z \quad , \qquad \tau_{xz}^0 = \frac{V_z}{A} = -\frac{M_y^{*'}}{A} \quad (5a, b)$$

Where τ_{xz}^0 represents the mean value of the shear stress and σ_{xx}^0 signifies initial normal stress in the cross section. Also, A and I_y are the cross-sectional area and the second moment of inertia about y-axis, are defined as follows:

$$A = \int_A dA, \quad I_y = \int_A z^2 dA \quad (6a, b)$$

2. 3. Equilibrium equations

The principle of minimum total potential energy is adopted herein to obtain equilibrium equations and boundary conditions. For beams with thin-walled section, the total potential energy Π is expressed by the summation of the elastic strain energy U_l and the strain energy due to initial stress U_0:

$$\delta\Pi = \delta(U_l + U_0) = 0 \quad (7)$$

δ is a variational symbol in the last formulation. Note that in the context of linear stability, where the beam is not under any external forces, one considers that the work done by external applied loads (W_e) equals to zero. δU_l could be computed using the following equations:

$$\delta U_l = \int_0^L \int_A \left(\sigma_{xx}\delta\varepsilon_{xx}^l + \tau_{xy}\delta\gamma_{xy}^l + \tau_{xz}\delta\gamma_{xy}^l\right)dA\,dx \quad (8)$$

in which, L expresses the element length and the cross-sectional area, respectively. $\delta\varepsilon_{xx}^l$, $\delta\gamma_{xz}^l$ and $\delta\gamma_{xy}^l$ are the variation of the linear parts of strain tensor. Substituting equations (4a) to (4c) into relation (8), the expression of the virtual elastic strain energy can be carried out as:

$$\delta U_l = \int_0^L \int_A \sigma_{xx}\left(\delta u_0' - y\,\delta v'' - z\,\delta w'' - \omega\delta\theta''\right)dA\,dx$$
$$+\int_0^L \int_A \tau_{xy}\left(-(z + \frac{\partial\omega}{\partial y})\delta\theta'\right)dA\,dx \quad (9)$$
$$+\int_0^L \int_A \tau_{xz}\left((y - \frac{\partial\omega}{\partial z})\delta\theta'\right)dA\,dx$$

Integrating over beam's cross-section area yields:

$$\delta U_l = \int_L \left(N\,\delta u_0' + M_z\,\delta v'' - M_y\,\delta w'' + B_\omega\delta\theta''\right)dx$$
$$+\int_0^L \left(M_{sv}\,\delta\theta'\right)dx \quad (10)$$

where N is the axial force. M_y and M_z denote the bending moments about major and minor axes, respectively. B_ω is the bi-moment. M_{sv} is the St-Venant torsion moment. These stress resultants used in Eq. (10) are defined as

$$N = \int_A \sigma_{xx}dA \quad (11a)$$

$$M_y = \int_A \sigma_{xx}zdA \quad (11b)$$

$$M_z = -\int_A \sigma_{xx}ydA \quad (11c)$$

$$B_\omega = -\int_A \sigma_{xx}\omega dA \quad (11d)$$

$$M_{sv} = \int\left(\tau_{xz}(y - \frac{\partial\omega}{\partial z}) - \tau_{xy}(z + \frac{\partial\omega}{\partial y})\right)dA \quad (11e)$$

Also, the variation of strain energy due to initial stresses can be stated as:

$$\delta U_0 = \int_0^L \int_A \left(\sigma_{xx}^0\delta\varepsilon_{xx}^* + \tau_{xy}^0\delta\gamma_{xy}^* + \tau_{xz}^0\delta\gamma_{xz}^*\right)dA\,dx \quad (12)$$

Inserting the first variation of non-linear strain-displacement relations defined in Eqs. (4d)-(4f) and initial stresses (5a, b) in Eq. (12), the following equation is obtained.

11

$$\delta U_0 = \int_0^L \int_A \left(\frac{P}{A} - \frac{M_y^*}{I_y}z\right)\begin{pmatrix} v'\delta v' + w'\delta w' \\ + r^2\theta'\delta\theta' + y\theta'\delta w' \\ + yw'\delta\theta' \\ - z\theta'\delta v' - zv'\delta\theta' \end{pmatrix} dA\,dx$$

$$+ \int_0^L \int_A \left(-\frac{M_y^{*'}}{A}\right)\left(-\theta\delta v' - v'\delta\theta - z\theta\delta\theta' - z\theta'\delta\theta\right)dA\,dx \tag{13}$$

In this stage, by integrating Eq. (13) over the cross-section in the context of principal axes, the final form of the variation of the strain energy due to the initial stresses is acquired as:

$$\delta U_0 = \int_0^L \left(P(v'\delta v' + w'\delta w' + \frac{I_y + I_z}{A}\theta'\delta\theta')\right)dx$$

$$+ \int_0^L \left(M_y^*(\theta'\delta v' + v'\delta\theta')\right)dx \tag{14}$$

$$+ \int_0^L \left(M_y^{*'}(\theta\delta v' + v'\delta\theta)\right)dx$$

Or

$$\delta U_0 = \int_0^L \left(Pv'\delta v' + Pw'\delta w' + r_o^2\theta'\delta\theta'\right)dx$$

$$+ \int_0^L \left(-M_y^* v''\delta\theta - M_y^*\theta\delta v''\right)dx \tag{15}$$

In Eq. (15), I_z is the second moment of inertia about z-axis and r_0 the polar radius gyration about the centroid given by:

$$I_z = \int_A y^2 dA, \quad r_o = \sqrt{\frac{I_y + I_z}{A}} \tag{16}$$

By inserting Eqs. (10) and (15) into Eq. (7) and setting the coefficients of $\delta u_0, \delta v, \delta w, \delta\theta$ zero, the following equilibrium equations are acquired:

$$N' = 0 \tag{17a}$$

$$-M_y'' - (Pw')' = 0 \tag{17b}$$

$$M_z'' - (M_y^*\theta)'' - (Pv')' = 0 \tag{17c}$$

$$B_\omega'' - M_y^* v'' - M_{sv}' - (Pr_O^2\theta')' = 0 \tag{17d}$$

Under the following boundary conditions:

$$N = 0 \qquad \text{or} \qquad \delta u_0 = 0 \tag{18a}$$

$$-M_y = 0 \qquad \text{or} \qquad \delta w' = 0 \tag{18b}$$

$$M_y' + Pw' = 0 \qquad \text{or} \qquad \delta w = 0 \tag{18c}$$

$$M_z - M_y^*\theta = 0 \qquad \text{or} \qquad \delta v' = 0 \tag{18d}$$

$$-M_z' + (M_y^*\theta)' + Pv' = 0 \qquad \text{or} \qquad \delta v = 0 \tag{18e}$$

$$B_\omega = 0 \qquad \text{or} \qquad \delta\theta' = 0 \tag{18f}$$

$$-B_\omega' + M_{sv} + Pr_O^2\theta' = 0 \qquad \text{or} \qquad \delta\theta = 0 \tag{18g}$$

The present model is applied in the case of balanced and symmetrical lay-ups of the web and both flanges. In the context of classical laminated plate theory and substitution Eq. (4) into Eq. (11), the stress resultants are derived in terms of displacement components as:

$$N = (EA)_{com} u_0' \tag{19a}$$

$$M_z = (EI_z)_{com} v'' \tag{19b}$$

$$M_y = -(EI_y)_{com} w'' \tag{19c}$$

$$B_\omega = (EI_\omega)_{com} \theta'' \tag{19d}$$

$$M_{sv} = (GJ)_{com} \theta' \tag{19e}$$

where $(EA)_{com}$ denotes axial rigidity. $(EI_y)_{com}$ and $(EI_z)_{com}$ represent the flexural rigidities of the y- and z-axes, respectively. $(EI_\omega)_{com}$ and $(GJ)_{com}$ are, respectively, warping and torsional rigidities of composite thin-walled beams with doubly symmetric I-section, defined by:

$$(EA)_{com} = (2b_f + (d - t_f))A_{11} \tag{20a}$$

$$(EI_z)_{com} = 2\frac{b_f^3}{12}A_{11} + dD_{11} \tag{20b}$$

$$(EI_y)_{com} = 2b_f D_{11} + 2\frac{(d - t_f)^2}{4}b_f A_{11}$$
$$+ \frac{(d - t_f)^3}{12}A_{11} \tag{20c}$$

$$(EI_\omega)_{com} = 2(\frac{d^2}{4}A_{11} + D_{11})\frac{b_f^3}{12} + \frac{d^3}{12}D_{11} \tag{20d}$$

$$(GJ)_{com} = 4(2b_f + d)D_{66} \tag{20e}$$

in which, A_{11} and D_{11}, D_{66} are the matrices of extensional and bending stiffness of each wall section, respectively, including the contribution from both the porous core and face layers, which are calculated as:

$$A_{11} = \frac{E_f}{1 - v_f^2}\int_{-0.5t_c - t_f}^{-0.5t_c} dz + \frac{E(x)}{1 - v^2}\int_{-0.5t_c}^{0.5t_c} dz$$
$$+ \frac{E_f}{1 - v_f^2}\int_{0.5t_c}^{0.5t_c + t_f} dz \tag{21a}$$

$$D_{11} = \frac{E_f}{1 - v_f^2}\int_{-0.5t_c - t_f}^{-0.5t_c} z^2 dz + \frac{E(x)}{1 - v^2}\int_{-0.5t_c}^{0.5t_c} z^2 dz$$
$$+ \frac{E_f}{1 - v_f^2}\int_{0.5t_c}^{0.5t_c + t_f} z^2 dz \tag{21b}$$

$$D_{66} = \frac{E_f}{2(1 + v_f)}\int_{-0.5t_c - t_f}^{-0.5t_c} z^2 dz + \frac{E(x)}{2(1 + v)}\int_{-0.5t_c}^{0.5t_c} z^2 dz$$
$$+ \frac{E_f}{2(1 + v_f)}\int_{0.5t_c}^{0.5t_c + t_f} z^2 dz \tag{21c}$$

where E_f and v_f are Young's modulus and Poisson's ratio of the face layers. E and v denote Young's moduli and Poisson's ratio of the porous core which are given in Eq. (1).

This study is established in the context of small displacements and deformations. According to linear stability, non-linear terms are also disregarded in the equilibrium equations. Based on these assumptions, the system of equilibrium equations for tapered I-beam are finally derived by replacing Eq. (19) into Eq. (17)

$$((EA)_{com}u_0')' = 0 \qquad (22a)$$

$$((EI_y)_{com}w'')'' - Pw'' = 0 \qquad (22b)$$

$$((EI_z)_{com}v'')'' - (M_y^*\theta)'' - Pv'' = 0 \qquad (22c)$$

$$((EI_\omega)_{com}\theta'')'' - ((GJ)_{com}\theta')' - M_y^*v'' \qquad (22d)$$

The related boundary conditions at the ends of thin-walled beam with I-section can be expressed as:

$$(EA)_{com}u_0' = 0 \qquad \text{or} \qquad \delta u_0 = 0$$

$$(EI_y)_{com}w'' = 0 \qquad \text{or} \qquad \delta w' = 0$$

$$((EI_y)_{com}w'')' - Pw' = 0 \qquad \text{or} \qquad \delta w = 0$$

$$(EI_z)_{com}v'' - M_y^*\theta = 0 \qquad \text{or} \qquad \delta v' = 0$$

$$\begin{aligned}&((EI_z)_{com}v'')' - (M_y^*\theta)'\\&-Pv' = 0\end{aligned} \qquad \text{or} \qquad \delta v = 0 \qquad (23)$$

$$(EI_\omega)_{com}\theta'' = 0 \qquad \text{or} \qquad \delta\theta' = 0$$

$$\begin{aligned}&((EI_\omega)_{com}\theta'')' - GJ\theta'\\&-M_y^*v' - (Pr_O^2\theta') = 0\end{aligned} \qquad \text{or} \qquad \delta\theta = 0$$

In the subsequent section, a numerical solution procedure of the governing equations for flexural-torsional buckling of sandwich tapered I-beam having AFG porous core is presented based on the differential quadrature method (DQM).

3. Solution Methodology

As aforementioned, the differential quadrature method is used to calculate the critical loads trough solving the couple fourth-order differential equations. According to DQM, the mth order derivative of a function $f(x)$ is described as:

$$\left.\frac{d^m f}{dx^m}\right|_{x=x_p} = \sum_{j=1}^{N} A_{ij}^{(m)} f(x_j) \quad for \quad i = 1, 2, ..., N \qquad (24)$$

where N signifies the number of grid points and $A_{ij}^{(m)}$ is the weighting coefficient for the mth-order derivative. Following the DQ rules, the first-order derivative weighting coefficient ($A_{ij}^{(1)}$) is derived as:

$$A_{ij}^{(1)} = \begin{cases} \dfrac{M(x_i)}{(x_i - x_j)M(x_j)} & for \quad i \neq j \\ -\displaystyle\sum_{k=1, k\neq i}^{N} A_{ik}^{(1)} & for \quad i=j \end{cases} \quad i,j = 1, 2, ..., N \quad (25)$$

Where $M(x)$ is:

$$M(x_i) = \prod_{j=1, j\neq i}^{N} (x_i - x_j) \quad for \quad i = 1, 2, ..., N \qquad (26)$$

The higher-order DQM weighting coefficients can be acquired from the first-order weighting coefficient as:

$$A_{ij}^{(m)} = A_{ij}^{(1)} A_{ij}^{(m-1)} \qquad 2 \leq m \leq N-1 \qquad (27)$$

The position of the sample points along x direction is also acquired via the Chebyshev-Gauss-Lobatto methodology as:

$$x_i = \frac{L}{2}\left[1 - \cos\left(\frac{i-1}{N-1}\pi\right)\right], \qquad (28)$$
$$if \quad 0 \leq x \leq L \qquad i = 1, 2, ..., N$$

In order to facilitate the solution of the stability equations by means of the differential quadrature approach, a non-dimensional variable ($\xi = x/L$) is introduced. By the expansion of Eqs. (22b) - (22c), and then applying the differential quadrature discretization to the non-dimensional form of the resultant equations, the following expressions are obtained:

$$(EI_y)_{com}(\xi_j)(\sum_{j=1}^{N}A_{ij}^{(4)}w_j) + (EI_y)''_{com}(\xi_j)(\sum_{j=1}^{N}A_{ij}^{(2)}w_j)$$
$$+2(EI_y)'_{com}(\xi_j)(\sum_{j=1}^{N}A_{ij}^{(3)}w_j) - L^2P(\sum_{j=1}^{N}A_{ij}^{(2)}w_j) = 0 \qquad (29a)$$

$$(EI_z)_{com}(\xi_j)(\sum_{j=1}^{N}A_{ij}^{(4)}v_j) + (EI_z)''_{com}(\xi_j)(\sum_{j=1}^{N}A_{ij}^{(2)}v_j)$$
$$+2(EI_z)'_{com}(\xi_j)(\sum_{j=1}^{N}A_{ij}^{(3)}v_j) - L^2P(\sum_{j=1}^{N}A_{ij}^{(2)}v_j)$$
$$-L^2M_y^*(\xi_j)(\sum_{j=1}^{N}A_{ij}^{(2)}\theta_j) - 2L^2M_y^{*'}(\xi_j)(\sum_{j=1}^{N}A_{ij}^{(1)}\theta_j)$$
$$-L^2M_y^{*''}(\xi_j)\theta_j = 0 \qquad (29b)$$

$$(EI_\omega)_{com}(\xi_j)(\sum_{j=1}^{N}A_{ij}^{(4)}\theta_j) + 2(EI_\omega)'_{com}(\xi_j)(\sum_{j=1}^{N}A_{ij}^{(3)}\theta_j)$$
$$+((EI_\omega)''_{com}(\xi_j) - L^2(GJ)_{com}(\xi_j))(\sum_{j=1}^{N}A_{ij}^{(2)}\theta_j)$$
$$-L^2(GJ)'_{com}(\xi_j)(\sum_{j=1}^{N}A_{ij}^{(1)}\theta_j) - PL^2R_o(\xi_j)(\sum_{j=1}^{N}A_{ij}^{(2)}\theta_j)$$
$$-PL^2R_o{}'(\xi_j)(\sum_{j=1}^{N}A_{ij}^{(1)}\theta_j) - L^2M_y^*(\xi_j)(\sum_{j=1}^{N}A_{ij}^{(2)}v_j) = 0 \qquad (29c)$$

In Eq. (29c), $R_o = r_0^2$. It is possible to express the quadrature analog of the mentioned above formulations in the following matrix form:

$$\left(\begin{bmatrix} [K_{ww}] & [0] & [0] \\ [0] & [K_{vv}] & [0] \\ [0] & [0] & [K_{\theta\theta}] \end{bmatrix}_{3N\times 3N} \right.$$
$$+ \begin{bmatrix} [P_{ww}] & [0] & [0] \\ [0] & [P_{vv}] & [0] \\ [0] & [0] & [P_{\theta\theta}] \end{bmatrix}_{3N\times 3N} \times \left\{ \begin{matrix} \{w\} \\ \{v\} \\ \{\theta\} \end{matrix} \right\}_{3N\times 1}$$
$$\left. + \begin{bmatrix} [0] & [0] & [0] \\ [0] & [0] & [M_{v\theta}] \\ [0] & [M_{\theta v}] & [0] \end{bmatrix}_{3N\times 3N} \right)$$
$$= \left\{ \begin{matrix} \{0\} \\ \{0\} \\ \{0\} \end{matrix} \right\}_{3N\times 1} \tag{30}$$

Where

$$[K_{ww}] = [a^1][A]^{(4)} + [b^1][A]^{(3)} + [c^1][A]^{(2)}$$
$$[P_{ww}] = -PL^2[A]^{(2)}$$
$$[K_{vv}] = [a^2][A]^{(4)} + [b^2][A]^{(3)} + [c^2][A]^{(2)}$$
$$[P_{vv}] = -PL^2[A]^{(2)}$$
$$[M_{v\theta}] = -[k^2][A]^{(2)} - [l^2][A]^{(1)} - [m^2] \tag{31}$$
$$[K_{\theta\theta}] = [a^3][A]^{(4)} + [b^3][A]^{(3)} + [c^3][A]^{(2)}$$
$$\qquad\qquad - [d^3][A]^{(1)}$$
$$[P_{\theta\theta}] = -PL^2([g^3][A]^{(2)} + [h^3][A]^{(1)})$$
$$[M_{\theta v}] = -[k^3][A]^{(2)}$$

in which

$$a^1_{jk} = ((EI_y)_{com}\big|_{\xi=\xi_j})\delta_{jk}$$
$$b^1_{jk} = (2(EI_y)'_{com}\big|_{\xi=\xi_j})\delta_{jk}$$
$$c^1_{jk} = ((EI_y)''_{com}\big|_{\xi=\xi_j})\delta_{jk}$$
$$a^2_{jk} = ((EI_z)_{com}\big|_{\xi=\xi_j})\delta_{jk}$$
$$b^2_{jk} = (2(EI_z)'_{com}\big|_{\xi=\xi_j})\delta_{jk} \tag{32}$$
$$c^2_{jk} = ((EI_z)''_{com}\big|_{\xi=\xi_j})\delta_{jk}$$
$$k^2_{jk} = (L^2 M_y^*\big|_{\xi=\xi_j})\delta_{jk}$$
$$l^2_{jk} = (2L^2 M_y^{*'}\big|_{\xi=\xi_j})\delta_{jk}$$
$$m^2_{jk} = (L^2 M_y^{*''}\big|_{\xi=\xi_j})\delta_{jk}$$

$$a^3_{jk} = ((EI_\omega)_{com}\big|_{\xi=\xi_j})\delta_{jk}$$
$$b^3_{jk} = (2(EI_\omega)'_{com}\big|_{\xi=\xi_j})\delta_{jk}$$
$$c^3_{jk} = (((EI_\omega)''_{com} - L^2(GJ)_{com})\big|_{\xi=\xi_j})\delta_{jk}$$
$$d^3_{jk} = (L^2(GJ)'_{com}\big|_{\xi=\xi_j})\delta_{jk}$$
$$g^3_{jk} = P((R_o)\big|_{\xi=\xi_j})\delta_{jk}$$
$$h^3_{jk} = P((R_o')\big|_{\xi=\xi_j})\delta_{jk}$$
$$k^3_{jk} = ((L^2 M_y^*)\big|_{\xi=\xi_j})\delta_{jk}$$

Here, δ_{jk} is Kronecker delta and defined as:

$$if\ ; j = k \Rightarrow \delta_{jk} = 1$$
$$if\ ; j \neq k \Rightarrow \delta_{jk} = 0 \tag{33}$$

In Eq. (30), the displacement vectors and the torsion angle vector are expressed as:

$$\{w\}_{N\times 1} = \{w_1 \quad w_2 \quad ... \quad w_N\}^T \tag{34a}$$
$$\{v\}_{N\times 1} = \{v_1 \quad v_2 \quad ... \quad v_N\}^T \tag{34b}$$
$$\{\theta\}_{N\times 1} = \{\theta_1 \quad \theta_2 \quad ... \quad \theta_N\}^T \tag{34c}$$

The simple form of the final equation (Eq. (25)) can be stated as:

$$([K] - \lambda([P] + [M]))_{3N\times 3N}\{d\}_{3N\times 1} = \{0\}_{3N\times 1} \tag{35}$$

or

$$([K] - \lambda[K_G])\{d\} = \{0\} \tag{36}$$

in which

$$[K_G] = [P] + [M]$$
$$\{d\} = \left\{ \begin{matrix} \{w\} \\ \{v\} \\ \{\theta\} \end{matrix} \right\} \tag{37a, b}$$

K and K_G are $3N \times 3N$ matrices. As mentioned previously, N denotes the number of grid points along the computation domain ($0 \leq \xi \leq 1$). λ are the eigenvalues and $\{d\}$ are the related eigenvectors. By imposing the boundary conditions at two ends, the flexural-torsional buckling loads are estimated through solving the eigenvalue problem.

4. Numerical Example

In the preceding section, a mathematical methodology has been formulated to calculate the flexural-torsional buckling loads of sandwich I-beam with varying cross-section. In this section, a comprehensive example is conducted to show the effects of significant parameters such as axial load position, power-law index, porosity volume fraction, thickness ratio (t_c/t_f) and non-uniformity parameter on the buckling capacity of sandwich doubly-symmetric web and flanges tapered I-beam having AFG porous core subjected to simply supported end conditions.

To this aim, the current section is divided to two different subsections; the first one for verification purpose of the formulation in the context of homogenous perfect tapered beam and the second one is devoted to perusing the influence of the above-mentioned factors on the linear buckling behavior of the considered member subjected to a compressive axial force at its ends.

In this benchmark example, it is supposed that the compressive axial load is applied at three different positions: the Top Flange (TF) of the left end section (x=0), the Centroid, and the TF of the right end section (x=L). It should be pointed out that the variations of flanges' width and web's height are identical to section 2.1 and Fig. 1. The geometrical data and loading positions for the considered beam are depicted in Fig. 2.

Material characteristics of sandwich porous beams with varying I-section which are stacked as steel/ axially functionally graded porous materials/steel with the following parameters:

Face layers: E_f=200GPa; $v_f = 0.3$.

AFG porous core: Al_2O_3: E_c=380GPa; Al: E_m=70GPa; $v = 0.3$.

To have a better understanding of the numerical outcomes, the evaluated flexural-torsional buckling load is presented in the non-dimensional form as:

$$P_{nor} = \frac{P_{cr}L^2}{E_f t d_L^3} \tag{38}$$
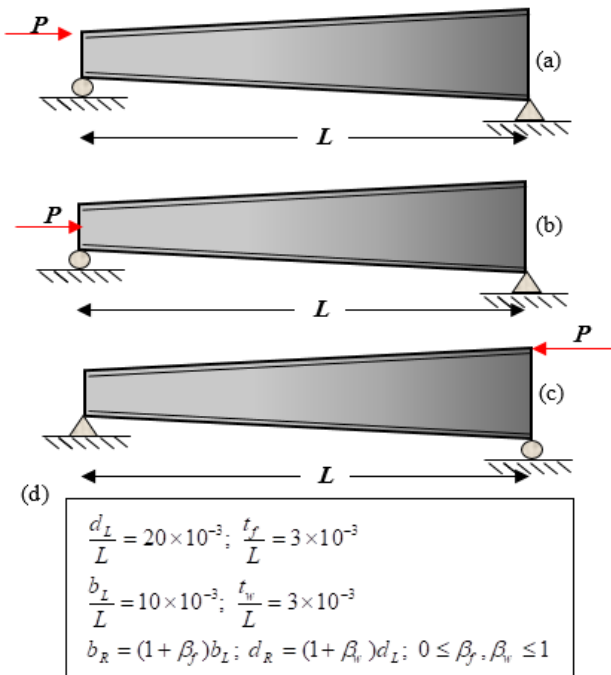
Fig. 2: Configuration of tapered I-beam with simply supported boundary condition, (a) Axial load on the TF of the left end section, (b) Axial load on the centroid, (c) Axial load on the TF of the right end section, (d) Geometry properties.

4.1. Verification

The aim of the first part of the current section is to define the needed number of points along the longitudinal direction while using DQM to obtain an acceptable accuracy on flexural-torsional buckling loads. In the absence of numerical studies on the subject of sandwich porous thin-walled beams, herein, the accuracy and exactness of the predicted results by the present formulation in the case of homogenous doubly-symmetric tapered beam are checked with those acquired by finite element technique proposed by Soltani et al. [38]. Regarding this, the lowest values of the non-dimensional buckling parameter (P_{nor}) of the contemplated beam with variable thin-walled I-section made of Alumina for two different loading positions and various values of tapering ratios ($\beta_f = \beta_w = 0$, 0.2, 0.5, and 0.8) are evaluated versus the number of sampling points adopted in DQ methodology. The resulting buckling parameters by the present formulation is depicted in Table 1.

Table 1: Convergence of the differential quadrature technique in determination of the lowest non-dimensional buckling load (P_{nor}) for tapered homogenous I-beam with different tapering parameters and loading positions.

Axial load position	$\beta_f = \beta_w$	DQM Number of points along x-direction				Soltani et al. [38]
		N=5	N=10	N=15	N=20	
Centroid	0	0.205	0.206	0.206	0.206	0.206
	0.2	0.270	0.271	0.271	0.271	0.272
	0.5	0.386	0.383	0.383	0.383	0.383
	0.8	0.530	0.511	0.511	0.511	0.511
TF of left end section	0	0.191	0.191	0.191	0.191	0.192
	0.2	0.247	0.247	0.247	0.247	0.248
	0.5	0.346	0.340	0.340	0.340	0.340
	0.8	0.475	0.442	0.442	0.442	0.443

It is seen from Table 1 that ten number of grid points (N=10) are sufficient to obtain the lowest normalized buckling loads for different axial load positions and non-uniformity parameters. Under this condition, for each case and load position, there is a good agreement between the proposed mathematical approach and those obtained by finite element solution developed by Soltani et al. [38].

4.2. Parametric Study

After the validation process of the present formulation for double-tapered I-section subjected to simply supported end conditions, the effects of significant parameters such as porosity volume fraction, the eccentric axial load, web and flanges tapering parameters and AFG power index (p),

on the flexural-torsional stability of sandwich thin-walled beam with AFG porous core are studied for $\frac{t_c}{t_f} = 10$.

In order to assess the linear stability strength of the sandwich AFG porous beam with varying I-section, the lowest normalized flexural-torsional buckling loads (P_{nor}) of considered I-beam subjected to simply supported end conditions are arranged in Table 2, which figures out the impact of web and flanges tapering ratios ($\beta_f = \beta_w = 0$, 0.2, 0.5, 0.8), material composition (power-law exponent), porosity volume fraction (α= 0 and 0.1) and three different loading positions on the buckling capacity of considered element. The compressive axial load can be applied on the TF of left end section (x=0), the centroid, and on the TF of right end section (x=L).

Table 2: Axial load eccentricity, gradient index and tapering parameter effect on the normalized buckling load (*P_{nor}*) of simply supported thin-walled beam subjected to constant compressive load with two different porosity volume fractions.

Loading Position	α	$\beta_f = \beta_w$	Material properties			
			Pure Ceramic	p=0.8	p=1.6	p=2.4
Axial load on the TF of left end section (x=0)	0	0.0	0.362	0.203	0.258	0.292
		0.2	0.467	0.272	0.346	0.388
		0.5	0.640	0.392	0.495	0.550
		0.8	0.833	0.529	0.663	0.732
	0.1	0.0	0.330	0.182	0.238	0.272
		0.2	0.425	0.245	0.319	0.362
		0.5	0.583	0.355	0.459	0.515
		0.8	0.758	0.482	0.617	0.686
Axial load on the centroid	0	0.0	0.396	0.215	0.277	0.315
		0.2	0.522	0.294	0.378	0.427
		0.5	0.737	0.435	0.555	0.623
		0.8	0.982	0.601	0.764	0.851
	0.1	0.0	0.360	0.192	0.254	0.292
		0.2	0.474	0.264	0.348	0.398
		0.5	0.670	0.392	0.513	0.582
		0.8	0.894	0.544	0.708	0.797
Axial load on the TF of right end section (x=L)	0	0.0	0.362	0.194	0.247	0.280
		0.2	0.462	0.256	0.324	0.366
		0.5	0.621	0.357	0.452	0.507
		0.8	0.792	0.469	0.592	0.661
	0.1	0.0	0.330	0.174	0.226	0.260
		0.2	0.421	0.230	0.298	0.341
		0.5	0.566	0.322	0.416	0.473
		0.8	0.721	0.424	0.547	0.618

Next, the influence of porosity volume fraction (ranging from 0 to 0.2) on the variations of the non-dimensional flexural-torsional buckling loads (P_{nor}) of sandwich thin-walled beam with varying I-section having pure ceramic or axially functionally materials core with different gradient indexes (p=1 and 3) with respect to tapering ratios (varying from 0 to 1.0) is plotted in Figs. 3-5 for three different loading positions. Load position of the constant compressive axial load is on the TF of the smaller cross-section (x=0), on the centroid and the TF of the larger cross-section (x=L). In this stage, the non-uniform beam having equal web height and flanges width tapering ratios ($\beta_f = \beta_w$) is perused.
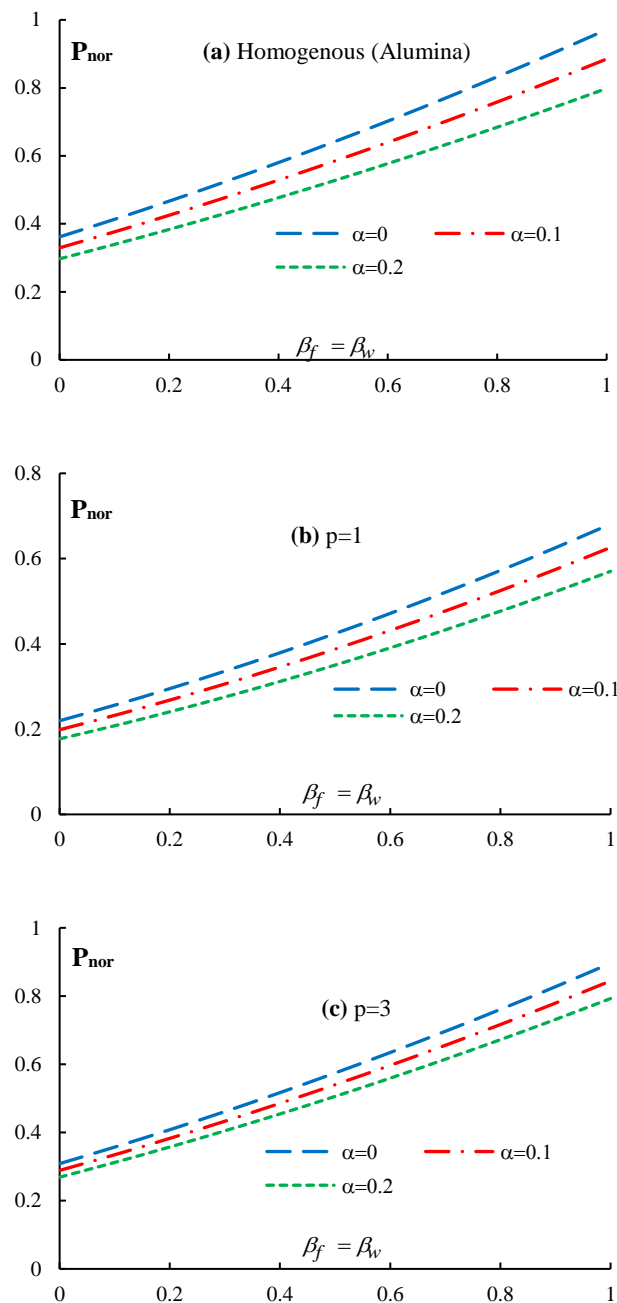
Fig. 3: Variation of the non-dimensional flexural-torsional buckling load (*P_{nor}*) of sandwich I-beam with tapering parameter and porosity volume fraction for different material indexes (axial load on the TF of left end section).
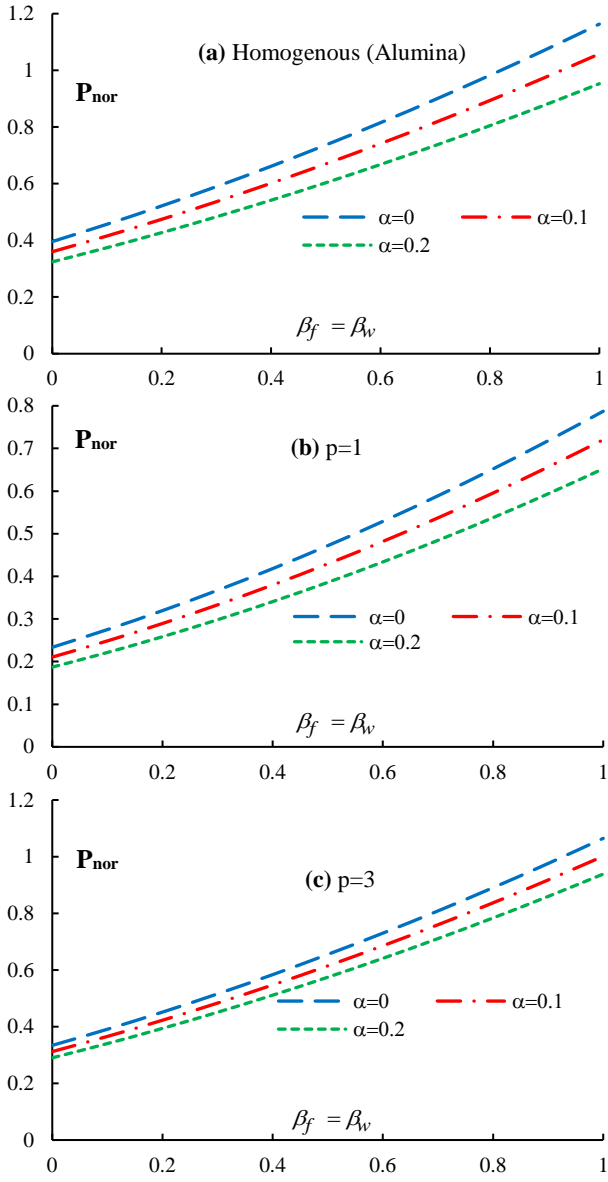
Fig. 4: Variation of the non-dimensional flexural buckling load (*P_{nor}*) of sandwich I-beam with tapering parameter and porosity volume fraction for different material indexes (axial load on the centroid).
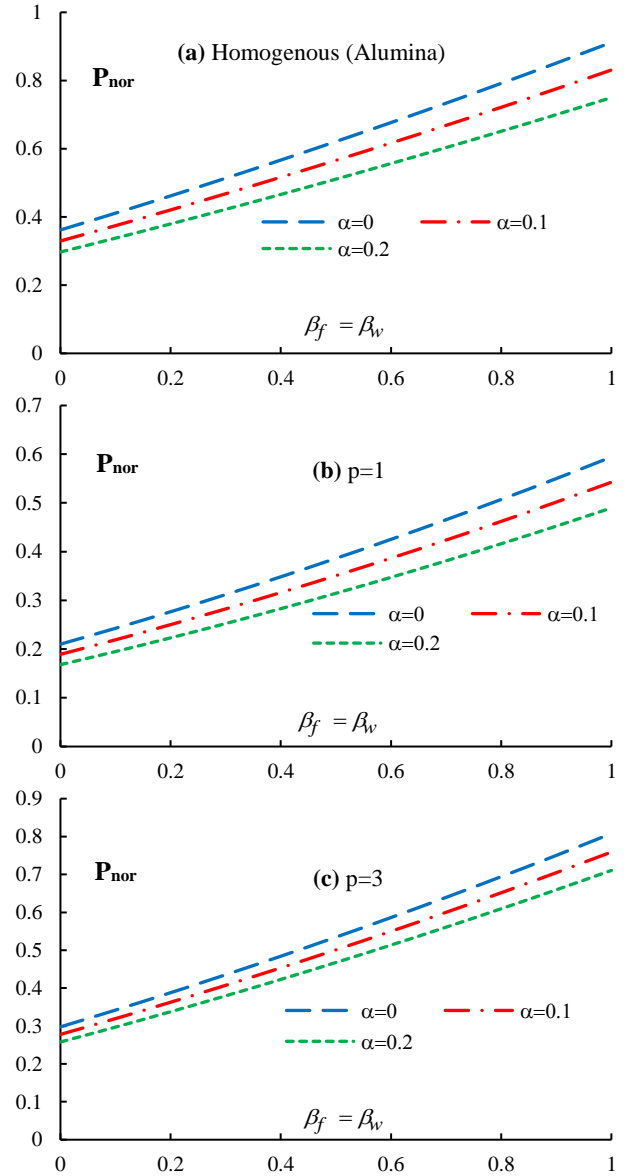
Fig. 5: Variation of the non-dimensional flexural-torsional buckling load (*P_{nor}*) of sandwich I-beam with tapering parameter and porosity volume fraction for different material indexes (axial load on the TF of right end section).

Table 3: Power-law exponent and tapering parameter effects on the normalized flexural-torsional buckling load (*P_{nor}*) of simply supported sandwich thin-walled beam with different porous parameters (axial load on the TF of left end section).

α	β_w	p=0.6			p=1.2			p=1.8		
		$\beta_f = 0$	$\beta_f = 0.4$	$\beta_f = 0.8$	$\beta_f = 0$	$\beta_f = 0.4$	$\beta_f = 0.8$	$\beta_f = 0$	$\beta_f = 0.4$	$\beta_f = 0.8$
	0	0.1839	0.3126	0.4638	0.2343	0.3983	0.5880	0.2684	0.4517	0.6608
0	0.4	0.1852	0.3162	0.4715	0.2362	0.4036	0.5990	0.2707	0.4582	0.6740
	0.8	0.1863	0.3193	0.4780	0.2377	0.4080	0.6081	0.2727	0.4636	0.6848
	0	0.1631	0.2798	0.4181	0.2134	0.3658	0.5429	0.2477	0.4198	0.6167
0.1	0.4	0.1642	0.2830	0.4248	0.2150	0.3706	0.5529	0.2499	0.4258	0.6289
	0.8	0.1651	0.2856	0.4304	0.2164	0.3745	0.5611	0.2516	0.4307	0.6388
	0	0.1417	0.2462	0.3712	0.1920	0.3327	0.4971	0.2268	0.3876	0.5721
0.2	0.4	0.1425	0.2487	0.3769	0.1934	0.3368	0.5060	0.2286	0.3930	0.5833
	0.8	0.1432	0.2509	0.3815	0.1945	0.3402	0.5133	0.2302	0.3974	0.5924

Table 4: Power-law exponent and tapering parameter effects on the normalized flexural-torsional buckling load (P_{nor}) of simply supported sandwich thin-walled beam with different porous parameters (axial load on the TF of right end section).

α	β_w	p=0.6			p=1.2			p=1.8		
		$\beta_f = 0$	$\beta_f = 0.4$	$\beta_f = 0.8$	$\beta_f = 0$	$\beta_f = 0.4$	$\beta_f = 0.8$	$\beta_f = 0$	$\beta_f = 0.4$	$\beta_f = 0.8$
	0	0.1771	0.3091	0.4743	0.2239	0.3930	0.6033	0.2566	0.4483	0.6848
0	0.4	0.1686	0.2925	0.4471	0.2125	0.3709	0.5679	0.2433	0.4229	0.6446
	0.8	0.1614	0.2786	0.4249	0.2030	0.3529	0.5395	0.2323	0.4023	0.6125
	0	0.1564	0.2750	0.4241	0.2031	0.3588	0.5533	0.2359	0.4145	0.6356
0.1	0.4	0.1489	0.2602	0.3997	0.1927	0.3386	0.5207	0.2236	0.3909	0.5982
	0.8	0.1426	0.2478	0.3799	0.1841	0.3222	0.4947	0.2135	0.3719	0.5684
	0	0.1350	0.2398	0.3726	0.1817	0.3239	0.5024	0.2149	0.3804	0.5859
0.2	0.4	0.1286	0.2269	0.3510	0.1725	0.3055	0.4726	0.2037	0.3586	0.5513
	0.8	0.1231	0.2161	0.3335	0.1647	0.2907	0.4489	0.1944	0.3412	0.5238

The magnitude of the normalized flexural-torsional buckling parameter (P_{nor}) for various combinations of web height and flange width tapering ratios (β_f and β_w), porosity volume fractions (α= 0, 0.1 and 0.2) with different in-homogenous indices (p=0.6, 1.2 and 1.8) are listed in Tables 3-4. The contribution of axial load eccentricity from the cross-section centroid on the buckling resistance is also taken into account. The resulting normalized buckling parameters are respectively illustrated in Tables 3 and 4 for load positions on the TF of smaller end-section and on the TF of right end-section.

The tables and figures indicate that non-uniformity parameter has a remarkable influence on the non-dimensional flexural-torsional buckling loads. It can be deduced that for any value of power-law exponents, porosity volume fraction and loading positions, the stability of prismatic beam ($\beta_w = \beta_f = 0$) and double tapered one with $\beta_w = \beta_f = 1$ is least and most, respectively. By pondering Tables 3-4 and Figs. 6-7, one can conclude that the effect of the rate of flanges width tapering parameter (β_f) is more than the effect of the web non-uniformity ratio (β_w). The reason is attributed to the fact that the lowest flexural-torsional buckling modes usually occur with respect to the minor axis moment of inertia.

According to the illustrations related to beams subjected to axial load on the centroid and on the TF of smaller end section, it is observed that the buckling parameter increases with an increase in web non-uniformity ratio (β_w), as a result of the enhancement of all geometrical characteristics of cross-section and consequently flexural stiffness and torsional rigidity of the elastic member. While the other results relating to I-beams with an axial load on the TF of right end section do not follow a similar pattern. As shown in Table 4, the linear stability strength of beams having constant flanges' width is diminished with web tapering ratio. For instance, the flexural-torsional buckling loads of perfect and porous I-beams with constant web height ($\beta_f = 0$) are larger than those of web-tapered with tapering ratio equals 1. This interesting reason is attributed to the fact that the initial bending moment (M_y^*) due to axial load eccentricity is enhanced by increasing the web tapering ratio (β_f) from zero. Finally, it can be stated that this phenomenon is negligible on the buckling resistance of web and flanges tapered beams when all section walls have a same non-uniformity ratio ($\beta_w = \beta_f$).

One remarks that for the three contemplated load cases, the buckling capacity is best when the axial load location is on the centroid and the lower values are obtained when the load is applied on the TF positions owing to the presence of the initial bending moment resulting by axial load eccentricity.

It is observable from these illustrations that the non-dimensional buckling load decreases by increasing the porosity due to decreasing the stiffness. Also, it is seen that a higher flexural-torsional buckling capacity is obtained by an increase in the power index (**p**). The reason is the higher portion of ceramic phase as the value of the gradient index rises.

The effect of thickness ratio t_c/t_f is then perused. Assuming that compressive load is located on the centroid, Figs. 6 illustrates the variation of the normalized buckling load with respect to the tapering parameter ($\beta_w = \beta_f$) for different thickness ratios. In this section, the flanges and web thicknesses are kept constant while both t_c and t_f are varied. It is necessary to point out that a larger thickness ratio matched with a sandwich I-beam which is closer to a functionally graded porous beam without metal face layers. Under this condition, the stiffness of the member is increased and consequently higher buckling load is obtained.
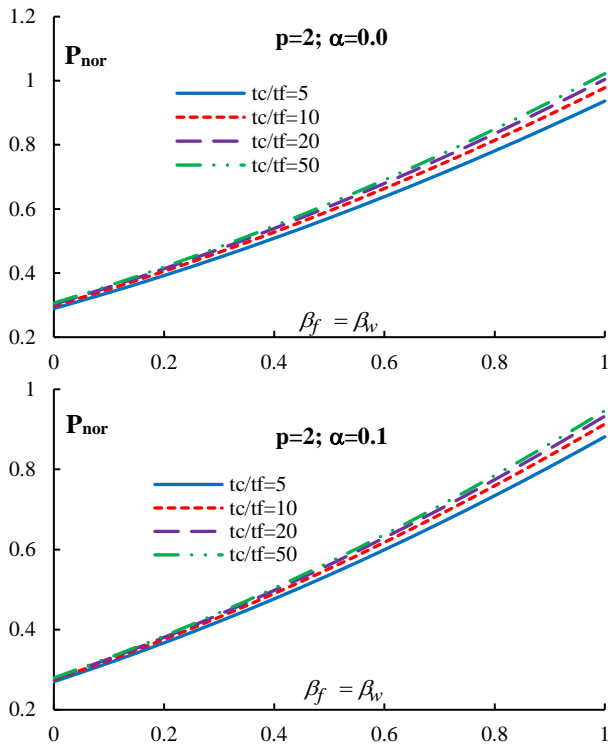
Fig. 6: Variation of the non-dimensional flexural-torsional buckling load (***P_nor***) of sandwich I-beam with tapering parameter and thickness ratio for different material indexes (axial load on the centroid).

5. Conclusions

In this manuscript, the effect of porosity on flexural-torsional buckling behavior of simply supported sandwich web and/or flanges tapered beam subjected to eccentrically compressive axial load was investigated. It is assumed that all section walls (the web and both flanges) are stacked as steel/ axially functionally graded porous materials/steel. Following the assumptions of Vlasov's theory and in the context of small displacement, the system of governing equilibrium equations is obtained using the energy method. As the resulting differential equations are strongly coupled in terms of the vertical and lateral displacements and the twist angle, the differential quadrature method is employed to estimate the critical buckling load. After verification, the influence of web and/or flanges tapering ratios, porosity volume fraction, thickness ratio, axial load position and axial variation of mechanical properties on flexural-torsional stability of sandwich I-beam is exhaustively surveyed. According to the numerical outcomes, it is concluded that the mentioned above parameters play significant roles in the stability strength of sandwich tapered I-beam having AFG porous core. It can be stated that the buckling capacity is best when the compressive axial load is applied on the centroid. It is illustrated that the non-dimensional buckling load increases by an increase in the percentage of ceramic phase. Additionally, it is

revealed that the increase in porosity volume fraction leads to decrease the buckling strength. By increasing the thickness of porous core, the stability strength is obviously enhanced. It is deduced that the effect of the flange tapering parameter (β_f) on the buckling capacity is more than the web tapering ratio (β_w).

References

[1] Rajasekaran, S. and Nalinaa, K., 2005. Stability and vibration analysis of non-prismatic thin-walled composite spatial members of generic section. *International Journal of Structural Stability and Dynamics*, *5*(04), pp.489-520. [2] Samanta, A. and Kumar, A., 2006. Distortional buckling in monosymmetric I-beams. *Thin-walled structures*, *44*(1), pp.51-56.

[3] Machado, S.P. and Cortínez, V.H., 2007. Free vibration of thin-walled composite beams with static initial stresses and deformations. *Engineering Structures*, *29*(3), pp.372-382.

[4] Kurniawan, C.W. and Mahendran, M., 2009. Elastic lateral buckling of simply supported LiteSteel beams subject to transverse loading. *Thin-Walled Structures*, *47*(1), pp.109-119.

[5] Ibanez, J.R. and Serna, M.A., 2010. Equivalent moment approach for elastic lateral-torsional buckling of tapered beams. *International Journal of Structural Stability and Dynamics*, *10*(03), pp.387-409.

[6] Yuan, W.B., Kim, B. and Chen, C.Y., 2013. Lateral–torsional buckling of steel web tapered tee-section cantilevers. *Journal of Constructional Steel Research*, *87*, pp.31-37.

[7] Li, X.F., Kang, Y.A. and Wu, J.X., 2013. Exact frequency equations of free vibration of exponentially functionally graded beams. *Applied Acoustics*, *74*(3), pp.413-420.

[8] Ebrahimi, F. and Mokhtari, M., 2015. Transverse vibration analysis of rotating porous beam with functionally graded microstructure using the differential transform method. *Journal of the Brazilian Society of Mechanical Sciences and Engineering*, *37*(4), pp.1435-1444.

[9] Jabbari, M., Mojahedin, A. and Joubaneh, E.F., 2015. Thermal buckling analysis of circular plates made of piezoelectric and saturated porous functionally graded material layers. *Journal of Engineering Mechanics*, *141*(4), p.04014148.

[10] Chen, D., Yang, J. and Kitipornchai, S., 2016. Free and forced vibrations of shear deformable functionally graded porous beams. *International journal of mechanical sciences*, *108*, pp.14-22.

[11] Chen, D., Kitipornchai, S. and Yang, J., 2016. Nonlinear free vibration of shear deformable sandwich beam with a functionally graded porous core. *Thin-Walled Structures*, *107*, pp.39-48.

[12] Saoula, A., Meftah, S.A. and Mohri, F., 2016. Lateral buckling of box beam elements under combined axial and bending loads. *Journal of Constructional Steel Research*, *116*, pp.141-155.

[13] Ebrahimi, F. and Jafari, A., 2016. A higher-order thermomechanical vibration analysis of temperature-dependent FGM beams with porosities. *Journal of Engineering*, *2016*.

[14] Shafiei, N. and Kazemi, M., 2017. Buckling analysis on the bi-dimensional functionally graded porous tapered nano-/micro-scale beams. *Aerospace Science and Technology*, *66*, pp.1-11.

[15] Khaniki, H.B. and Rajasekaran, S., 2018. Mechanical analysis of non-uniform bi-directional functionally graded intelligent micro-beams using modified couple stress theory. *Materials Research Express*, *5*(5), p.055703.

[16] Lezgy-Nazargah, M., Vidal, P. and Polit, O., 2013. An efficient finite element model for static and dynamic analyses of functionally graded piezoelectric beams. *Composite Structures*, *104*, pp.71-84.

[17] Lezgy-Nazargah, M. and Farahbakhsh, M., 2013. Optimum material gradient composition for the functionally graded piezoelectric beams. *International Journal of Engineering, Science and Technology*, *5*(4), pp.80-99.

[18] Lezgy-Nazargah, M., 2015. Fully coupled thermo-mechanical analysis of bi-directional FGM beams using NURBS isogeometric finite element approach. *Aerospace Science and Technology*, *45*, pp.154-164.

[19] Lezgy-Nazargah, M., 2017. A generalized layered global-local beam theory for elasto-plastic analysis of thin-walled members. Thin-Walled Structures, 115, pp.48-57.

[20] Lezgy-Nazargah, M. and Meshkani, Z., 2018. An efficient partial mixed finite element model for static and free vibration analyses of FGM plates rested on two-parameter elastic foundations. *Struct Eng Mech*, *66*, pp.665-676.

[21] Lezgy-Nazargah M, Vidal P, Polit O. A penalty-based multifiber finite element model for coupled bending and torsional-warping analysis of composite beams. European Journal of Mechanics-A/Solids. 2020; 80:103915.

[22] Tang, H., Li, L. and Hu, Y., 2018. Buckling analysis of two-directionally porous beam. *Aerospace Science and Technology*, *78*, pp.471-479.

[23] Nguyen, N.D., Nguyen, T.K., Vo, T.P., Nguyen, T.N. and Lee, S., 2019. Vibration and buckling behaviours of thin-walled composite and functionally graded sandwich I-beams. *Composites Part B: Engineering*, *166*, pp.414-427.

[24] Koutoati, K., Mohri, F. and Daya, E.M., 2019. Finite element approach of axial bending coupling on static and vibration behaviors of functionally graded material sandwich beams. *Mechanics of Advanced Materials and Structures*, pp.1-17.

[25] Ghasemi, A.R. and Meskini, M., 2019. Free vibration analysis of porous laminated rotating circular cylindrical shells. *Journal of Vibration and Control*, *25*(18), pp.2494-2508.

[26] Achref, H., Foudil, M. and Cherif, B., 2019. Higher buckling and lateral buckling strength of unrestrained and braced thin-walled beams: Analytical, numerical and design approach applications. *Journal of Constructional Steel Research*, *155*, pp.1-19.

[27] Rajasekaran, S. and Khaniki, H.B., 2019. Bi-directional functionally graded thin-walled non-prismatic Euler beams of generic open/closed cross section Part I: Theoretical formulations. *Thin-Walled Structures*, *141*, pp.627-645.

[28] Asgarian, B., Soltani, M. and Mohri, F., 2013. Lateral-torsional buckling of tapered thin-walled beams with arbitrary cross-sections. *Thin-walled structures*, *62*, pp.96-108.

[29] Soltani, M., Asgarian, B. and Mohri, F., 2014. Elastic instability and free vibration analyses of tapered thin-walled beams by the power series method. *Journal of constructional steel research*, *96*, pp.106-126.

[30] Soltani, M., Asil Gharebaghi, S. and Mohri, F., 2018. Lateral stability analysis of steel tapered thin-walled beams under various boundary conditions. *Journal of Numerical Methods in Civil Engineering*, *3*(1), pp.13-25.

[31] Soltani, M., Asgarian, B. and Mohri, F., 2019. Improved finite element model for lateral stability analysis of axially functionally graded nonprismatic I-beams. *International Journal of Structural Stability and Dynamics*, *19*(09), p.1950108.

[32] Soltani, M. and Asgarian, B., 2020. Lateral-Torsional Stability Analysis of a Simply Supported Axially Functionally Graded Beam with a Tapered I-Section. *Mechanics of Composite Materials*, pp.1-16.

[33] Soltani, M. and Asgarian, B., Exact stiffness matrices for lateral–torsional buckling of doubly symmetric tapered beams with axially varying material properties, DOI: 10.1007/s40996-020-00402-z.

[34] Yang, Y.Y. and Munz, D., 1997. Stress analysis in a two materials joint with a functionally graded material. In *Functionally Graded Materials 1996* (pp. 41-46). Elsevier Science BV.

[35] Jin, Z.H. and Paulino, G.H., 2001. Transient thermal stress analysis of an edge crack in a functionally graded material. *International Journal of Fracture*, *107*(1), pp.73-98.

[36] Delale, F. and Erdogan, F., 1983. The crack problem for a nonhomogeneous plane.

[37] ZJin, Z.H. and Noda, N., 1994. Crack-tip singular fields in nonhomogeneous materials.

[38] Soltani, M., Asgarian, B. and Mohri, F., 2014. Finite element method for stability and free vibration analyses of non-prismatic thin-walled beams. *Thin-Walled Structures*, *82*, pp.245-261.